J Mater Sci (2013) 48:6341–6351
DOI 10.1007/s10853-013-7433-3

Optical properties of vanadium oxides-an analysis

Chiranjivi Lamsal · N. M. Ravindra

Received: 21 February 2013 / Accepted: 6 May 2013 / Published online: 16 May 2013

Abstract In this study, the optical properties of bulk and thin films of VO_2, V_2O_3, and V_2O_5, deposited on Al_2O_3 substrates, have been analyzed from infrared to vacuum ultraviolet range (up to 12 eV). Utilizing the available data of wavelength dependent optical constants of these materials in the literature, the energy corresponding to the peaks in the imaginary part of the dielectric function (ε_2–R spectra), have been interpreted and compared as a function of structure, polarization, and temperature. The energies corresponding to the peaks in reflectivity-energy (R–E) spectra are explained in terms of the Penn gap (E_p). E_p values for VO_2 and V_2O_5 are close to the average of energies corresponding to the peaks ($\bar{E}$) while, their values are even closer in V_2O_3, reflecting the degree of anisotropy in the order of $V_2O_3 < VO_2 < V_2O_5$. The first order reversible, insulator to metal phase transition (IMT) of both bulk and thin films of the V–O systems are studied as an effect of temperature change. The effective number of electrons, n_{eff}, participating in the optical transitions is described from the numerical integration using the well-known sum rule. The change in n_{eff} with respect to the energy of incident photons is also calculated and it is found that this change is consistent with the peaks observed in the ε_2–E spectra.

Introduction

Vanadium is a d-transition metal having different oxidation states, and forms the so-called Magnéli (V_nO_{2n-1}) and Wadsley ($V_{2n}O_{5n-2}$) homologous series of vanadium–oxygen (V–O) systems. In the present study, we have analyzed the optical properties of V_2O_3 ($n = 2$) and VO_2 ($n = \infty$), which are the two end members of Magnéli phases and V_2O_5 ($n = \infty$), the end member of Wadsley phases. Vanadium ions in VO_2 and V_2O_3 have $V^{4+}(d^1)$ and $V^{3+}(d^2)$ electronic structures, respectively, whereas, V_2O_5 has V^{5+} ion with no 3d electrons. In these transition metal oxides, d electrons are spatially confined in partially filled orbitals and are considered to be strongly interacting or "correlated" because of Coulombic repulsion. Correlated electrons are responsible for the extreme sensitivity of materials for small change in external stimuli such as pressure, temperature, or doping [1].

Several vanadium oxides undergo insulator-metal transitions (IMT) at a particular temperature, T_c. The IMT, occurring in these materials, varies over a wide range of temperatures and depends on the O/V ratio [2]. Among them, VO_2 is one of the widely studied materials which undergoes IMT at 340 K [3], while V_2O_3 and V_2O_5 exhibit the transitions at 160 K [4] and 530 K [5], respectively. In recent days, the phase transition in bulk V_2O_5 has become a controversial issue even though the studies on its thin film show IMT; various transition temperatures have been reported for these materials in the literature [6, 7]. Furthermore, precise mechanism of IMT is still a matter of debate [8], and no theoretical understanding has been realized to predict the transition temperature [9].

These first order phase transitions are reversible [10] and are accompanied by drastic change in crystallographic, magnetic, optical and electrical properties. During structural transition, atoms undergo displacement with redistribution of electronic charge in the crystal lattice and hence, the nature of interaction changes [11]. Below T_c, the V–O system shows insulating behavior, wherein VO_2 and V_2O_3

C. Lamsal · N. M. Ravindra (✉)
Department of Physics, New Jersey Institute of Technology, Newark, NJ 07102, USA
e-mail: nmravindra@gmail.com

have monoclinic structure [12, 13] and V_2O_5 has orthorhombic structure [14]. At temperatures greater than T_c, they behave like metal, but with different crystal structures from their low temperature counterparts [12, 15]. However, Kang et al. [7] have concluded that V_2O_5 films undergo IMT without structural phase transition. Similarly, the phase transition leads to the change in electrical conductivity up to 10 orders of magnitude [16], while optical and magnetic properties show discontinuity.

The vanadium oxides are chromogenic materials and can change their optical properties due to some external stimuli in the form of photon radiation (photochromic), change in temperature (thermochromic) and voltage pulse (electrochromic); the change becomes discontinuous during IMT. Such properties can be exploited to make coatings for energy-efficient "smart windows" [17], and electrical and optical switching devices [18]. Thin films of VO_2 and V_2O_3 have been found to show good thermochromism in the infrared region [19, 20]. While maintaining the transparency to visible light, a smart window modulates infrared irradiation from a low-temperature transparent state to a high-temperature opaque state [21]. The two oxides, VO_2 and V_2O_5, can change their optical properties in a persistent and reversible way in response to a voltage [22]. V_2O_5 exhibits exceptional electrochromic behavior because it has both anodic and cathodic electrochromism, different from VO_2 which only has anodic electrochromism, and is also an integral part in band structure effects [22]. These electrochromic materials have four main applications: information displays, variable-reflectance mirrors, smart windows, and variable-emittance surfaces.

The V–O systems are widely applicable in technology such as memory devices and temperature sensors [23]. The memory aspect of the material is evidenced from the pronounced hysteresis present in phase transition [24]. Normally the range of operation of a device lies outside the hysteresis region. However, some bolometric devices are operational within the hysteretic transition [25]. Bolometers are thermal infrared (IR) detectors and can be used in infrared imaging applications such as thermal camera, night vision camera, surveillance, mine detection, early fire detection, medical imaging, and detection of gas leakage. A bolometer requires a material with high temperature coefficient of resistance (TCR) and a small $1/f$ noise constant [26]. Pure, stoichiometric single-crystals of VO_2 and V_2O_5 have high TCR but are difficult to grow. Furthermore, the latent heat involved in IMT is highly unfavorable for the bolometric performance [27]. Since T_c of V_2O_3 is far below room temperature, the resistance and hence, the level of noise is low which makes V_2O_3 a good candidate for the fabrication of efficient micro-bolometers. However, Cole et al. [28] have shown that the thin films of all the three oxides, combined together, can produce a desired material with high TCR and optimum resistance for bolometer fabrication.

Clearly, phase transition in VO_2 is of high technological interest. IMT occurs near to room temperature and T_c can be tuned optically, thermally, electrically [29], and with doping [16]. The phase transition in VO_2 has been used to achieve frequency-tunable metamaterials in the near-infrared range [30, 31]. Recently, Kyoung et al. [32] have extended the study to terahertz range proposing an active terahertz metamaterial, a gold nano-slot antenna on a VO_2 thin film, which transforms itself from transparent to complete extinct at resonance when the VO_2 film undergoes thermo or photoinduced phase transition. Cavalleri et al. [12] showed that the phase transition can be photoinduced within hundreds of femtoseconds, which can be an underlying principle for an ultrafast switch.

Vanadium dioxide (VO_2) [19, 33] and vanadium sesquioxide (V_2O_3) [34, 35] are the model systems used to study IMT in correlated electron systems. V_2O_5 is the most stable among the other two and exhibits highly anisotropic optoelectronic properties [7, 36]. While the study of vanadium-oxide systems is an exciting field of research due to its significant technological applications, the phase transition, high sensitivity to microscopic details, and anisotropic nature make the study more difficult. In general, the conventional band theory, which treats the electrons as extended plane waves, can explain the metallic behavior of a material, but fails to account for the localized electrons [37]. In transition metal oxides, the d electrons are partially localized and partially itinerant [38] and, during IMT, an electron changes its behavior from localized to itinerant. Even though the Mott–Hubbard transition (strong electron–electron interactions) and the Peierls mechanisms (electron–phonon interactions) are considered to be responsible for IMT, no general consensus has been reached amongst the scientific community [39]. Coping with such a transition problem, which involves understanding the "competition" between kinetic (wavelike) and correlation (particle like) terms in the electronic level, is still an exciting field of research and is the heart of electronic many body problems.

The optical property of a material originates from the response of electrons to perturbation due to the incident radiation and transition between electronic states. Electronic properties and energy band structure of a solid are effectively studied on the basis of its optical properties. Particularly, the frequency dependent complex refractive index and dielectric function are related to the electronic structure and band structure of the solid. Owing to the phase transition along with inherent drastic changes in the optical properties of the materials and inconsistent explanation of the phenomenon, the band gap calculation and absorption edge estimation have been of immense interest. Band gaps of VO_2 and V_2O_5, at room temperature, have been reported as 0.6 eV [2] and 2.3 eV [40], respectively, while a gap of 0.66 eV is found in V_2O_3 at 70 K [41]. In this study, we have mainly analyzed the spectral dependence of the complex dielectric function $\varepsilon(\omega)$ of both bulk and thin film of the V–O systems deposited on Al_2O_3 substrates, based on the data available in the literature. Observed peaks in the corresponding spectra have been interpreted and compared as a function of structure, polarization, and temperature. Complex dielectric function $\varepsilon(\omega)$ is related to the complex refractive index by the following equations:

$$\varepsilon_1 = n^2 - k^2 \quad (1)$$

and

$$\varepsilon_2 = 2nk \quad (2)$$

where, $n(\omega)$ and $k(\omega)$ are frequency (ω) dependent refractive index (n) and extinction coefficient (k) respectively.

Since the dielectric function is a complicated function of frequency [42], we have used the Penn model, a simplified model of a semiconductor or insulator [43, 44] to account for the average isotropic energy gap in terms of the long-wavelength electronic dielectric constant in the non-dispersive region. The results of Penn model are consistent within the degree of anisotropy in the order of $V_2O_3 < VO_2 < V_2O_5$. Van Vechten's [45] extension of Penn model to d-electrons has also been implemented to account for the energy gap, and ionicity of the bonds have been calculated using the empirical theory developed by Phillips [46]. Also, the sum rule has been applied to the V–O system to describe the effective number of electrons participating in the optical transitions.

Review of optical spectra

Above T_c, VO_2 has a tetragonal crystal structure with two distinct directions for electric polarization. The lower symmetry monoclinic structure is energetically favorable for the crystal phase below T_c, and hence higher degree of anisotropic behavior is expected with three distinct directions for electric polarization. However, the "domain" pattern [47], observed in this low temperature phase, reduces the degree of anisotropy and hence, electric vector (**E**) sees only two independent directions. Therefore, the optical properties have been studied with $\mathbf{E}\perp a$ axis for monoclinic phase and $\mathbf{E}\perp c$ axis for tetragonal phase and their parallel counter-parts. Anisotropic character of V_2O_3 is rarely taken into consideration, since experimental study of its electrical and optical properties show very small directional dependence [48, 49]. However, V_2O_5 is highly anisotropic [50].

By definition, dielectric function of an insulator or semiconductor quantifies the dielectric polarization, which in turn is described classically by the oscillation of a spring connecting a pair of electric charges generated by the external electric field. Resonant oscillation of the spring, followed by light absorption, can be observed when the frequency of the incident radiation matches with the oscillating frequency of the spring. In other words, ε_2, which is proportional to the amount of light absorbed in the medium, shows a peak corresponding to the resonance frequencies of the spring. Since the region of interest for incident photons lies within the infrared to the vacuum ultraviolet range, we will analyze, in essence, the atomic and electronic polarization. On the other hand, refraction or absorption of light in a medium can be completely determined by the complex refractive index, ($n + ik$), as well. Clearly, the real part (n) controls the speed of light in the medium while the extinction coefficient (k) signifies absorption and modulates the amplitude of the electromagnetic radiation in the medium.

Figures 1, 2, 3 and 4 show the variations in optical properties such as ε_1, ε_2, n, k, and R of the bulk and thin film of VO_2, V_2O_3, and V_2O_5 with photon energy at different temperatures and polarizations of electric field. It is evident from the figures that the optical parameters show strong variation with energy of incident photons from infrared to vacuum ultraviolet range (up to 12 eV). The value of ε_1 at temperature higher than T_c decreases with frequency at the lower end of the spectrum and becomes negative, while the ε_2–E spectra show the corresponding exponential increase with decrease in frequency. This can be attributed to the free-carrier absorption or Drude tail of the metallic [51] phase and can further be justified by the rapid increase in reflectivity spectra with decrease in frequency below $\omega < \omega_p$, the plasma frequency at which ε_1 becomes zero. The Drude absorption feature can also be observed in k–E spectra at high temperature metallic phase as evidenced in Fig. 3b. The anisotropy is manifested from the amplitude, width and energy position of the corresponding structure in the optical spectra for polarizations parallel to the crystallographic axes a, b, and c. By comparing the peaks in the ε_2–E spectra of insulating phase, for instance, of all the three oxides, V_2O_5 shows high anisotropic behavior; most of the peaks are more sharply peaked in V_2O_5 than those seen in VO_2 and V_2O_3. Similarly, unlike in high temperature phase, the absorption peaks in ε_2–E spectra, at low temperature phase, are relatively sharper. Clearly, temperature dependence of the spectral variation of the optical properties is highly manifested at the lower end of the spectrum. These changes in the infrared region during IMT are due to the onset of free carrier dominated absorption, a characteristic of metallic phase [47]. However, no remarkably high qualitative difference is observed in the optical spectrum between different temperatures at the higher frequency.

Figure 1 shows the comparison of reflectivity spectra and dielectric function—both real and imaginary part—of vanadium dioxide in the energy range of 0.25–5.0 eV as a function of temperature below and above T_c. Figure 1a, b shows ε_1–E, ε_2–E, and R–E spectra of bulk single crystal of VO_2 for polarization $\mathbf{E}\|a$ axis and $\mathbf{E}\perp a$ axis, respectively, while Fig. 1c shows the optical spectrum for 1000 Å polycrystalline thin film of VO_2 deposited on Al_2O_3 substrate. The band gap absorption, as expected in the ε_2–E spectra, cannot be seen which might be due to stoichiometric impurity and other imperfections of the samples. Comparison of Fig. 1a, b indicates the direction dependence of optical properties; absorption and reflectivity peaks, observed in the low temperature phase, are higher for the polarization $\mathbf{E}\perp a$ axis as compared to the parallel counterparts. Contribution of atomic polarization to the dielectric function, which is indicated by the first resonance peak located in the infrared region, at 300 K for electric field $\mathbf{E}\perp a$ axis is higher than for the polarization $\mathbf{E}\|a$ axis. A small peak appearing near 0.6 eV in the ε_1–E spectra in the metallic phase at 355 K, as seen in Fig 1b, is absent for the polarization $\mathbf{E}\|a$ axis. It means the anisotropy is remarkable in the infrared region. No significant difference in structural feature between the bulk and thin film spectra is seen. The structures in the spectra below 2.0 eV at high temperature phase have been described as a result of metallic free carrier dominated absorption [47]. However, significant peaks can be seen at energies above 2.5 eV in both phases, as indicated in Table 1, and are explained in terms of (direct) inter band transitions, i.e., the transitions between the 2p (O) and 3d (V) bands which are separated approximately by 2.5 eV [47]. A shoulder appearing relatively distinct near 0.7 eV in the ε_2–E spectra of high temperature phase, in Fig. 1b, has been interpreted as inter band transition within the 3d bands [47].

Figure 2 shows the reflectivity spectra and dielectric function-both real and imaginary part-of vanadium sesquioxide (V_2O_3) from infrared to vacuum ultraviolet range (up to 10.0 eV) as a function of temperature below and above T_c. Figure 2a shows the ε_1–E and ε_2–E spectra of bulk V_2O_3 calculated using density function theory [52] and R–E spectra of single crystal of V_2O_3 at near-normal incidence [34]. The absorption, in bulk V_2O_3 at temperature of 148 K, starts at 1 eV as seen in the ε_2–E spectra of Fig. 2a. It means that the low temperature insulating phase is transparent to infrared radiation. Other absorption peaks appear at near infrared, visible and near ultraviolet regions as indicated in Table 2. The highest but wider peak centered at 6.1 eV covers the range from 5 to 9 eV, which is

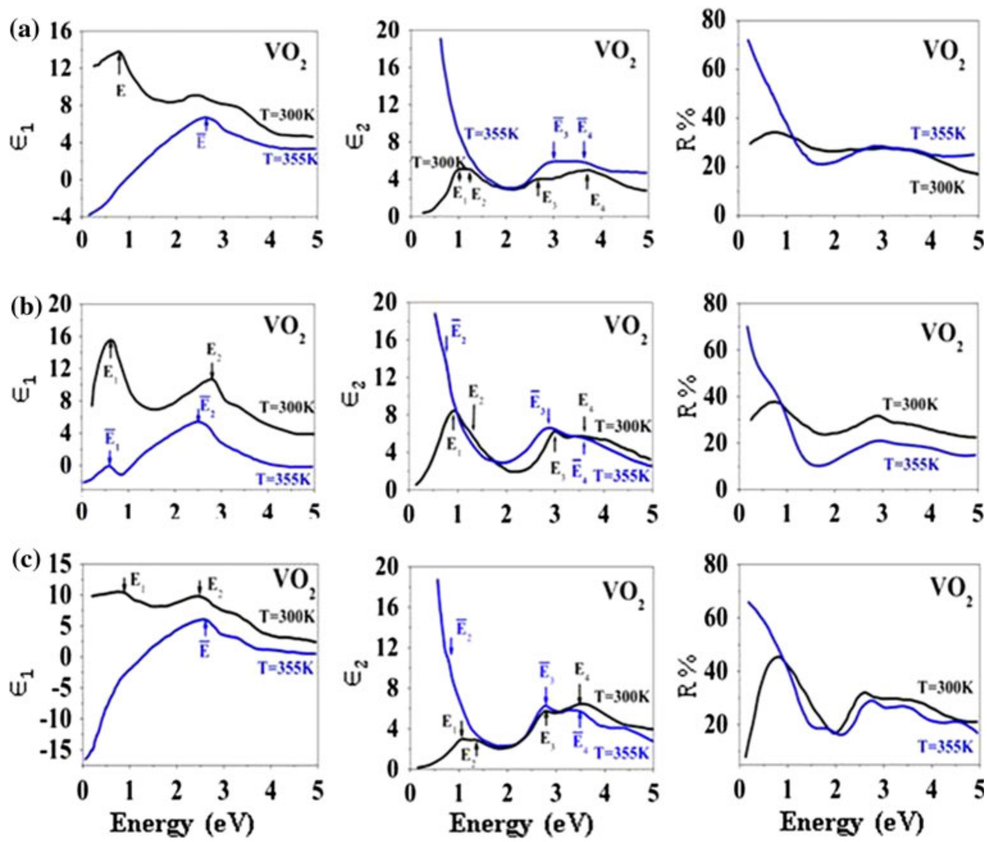

Fig. 1 Variation of ε_1, ε_2, and R with photon energy at temperatures 300 and 355 K [47] for bulk VO_2 with two polarizations of electric field **a** $\mathbf{E}\|a$ axis **b** $\mathbf{E}\perp a$ axis and **c** a 1000 Å thin film on Al_2O_3 (Color figure online)

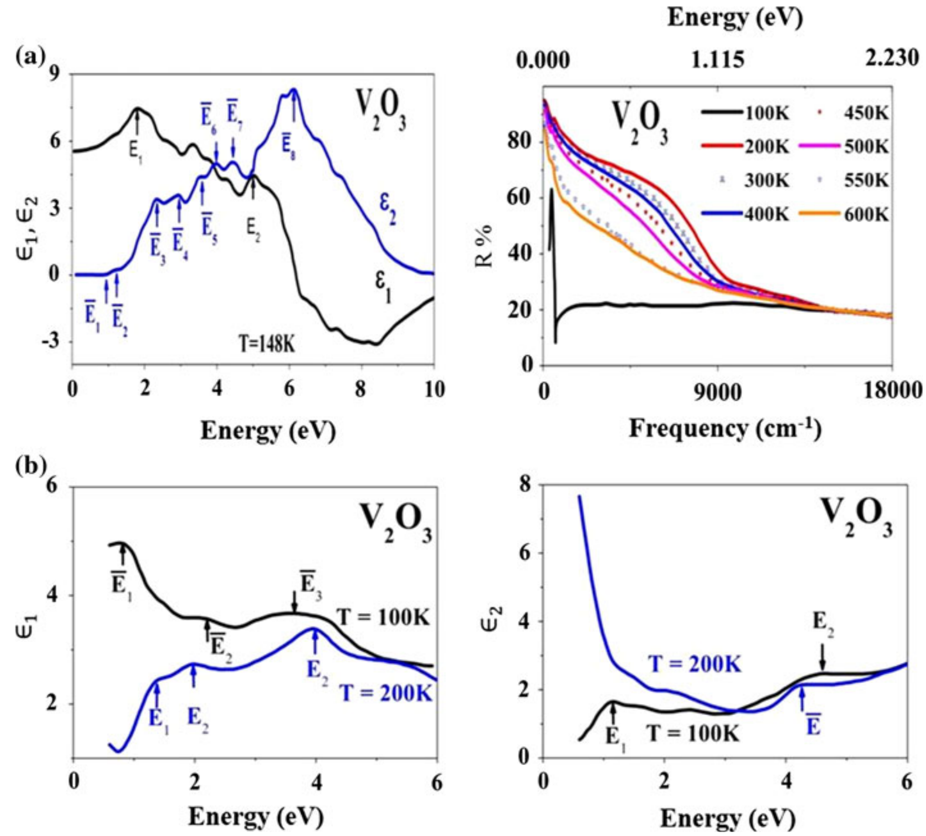

Fig. 2 Variation of ε_1, ε_2, and *R* with photon energy for **a** bulk V_2O_3 at different temperatures [34, 52] **b** thin film of V_2O_3 on Al_2O_3 substrate [53] (Color figure online)

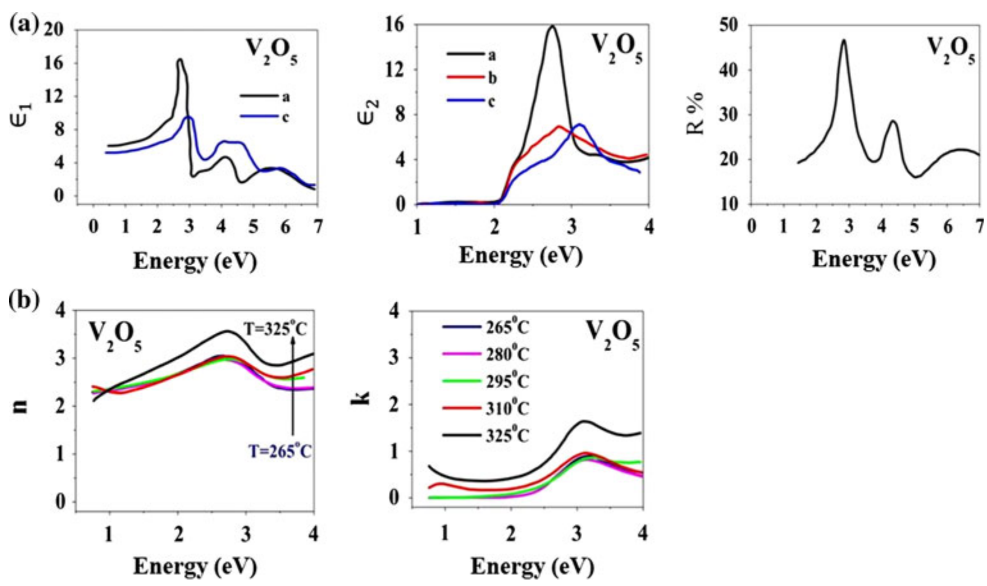

Fig. 3 Variation of ε_1 [54], ε_2 [50], *R*[54] *n*, and *k* [7] with photon energy for **a** bulk V_2O_5 at polarization **E**||*a* (*black*), **E**||*b* (*red*) and **E**||*c* (*blue*) **b** thin film of V_2O_5 on Al_2O_3 substrate (Color figure online)

an indication of strong absorption in the ultraviolet region. The infrared reflectivity spectra of a single crystal of V_2O_3, measured in the temperature range of 100–600 K, show two distinct behaviors. Unlike the *R*–*E* spectra at the temperature of 100 K, the reflectivity at low frequency edge increases with decrease in frequency at all temperatures above 200 K. This can be attributed to the high temperature metallic behavior. However, the temperature dependent variations at higher temperatures are relatively insignificant and it seems that the significant changes in reflectivity occur within a few degree of T_c. On the other hand, the high frequency reflectivity tails merge with each other, irrespective of the temperature. Figure 2b shows the dielectric function of a 75 nm polycrystalline film of V_2O_3 deposited on Al_2O_3 substrate at temperatures below and above T_c [53]. Table 2 lists the absorption peaks observed

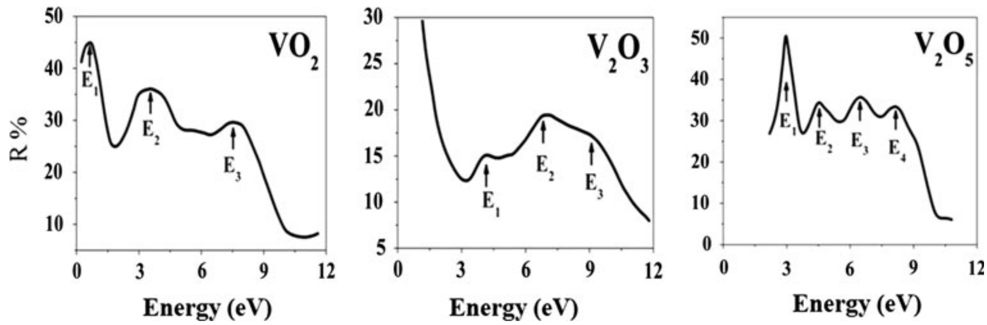

Fig. 4 Variation of R with photon energy for bulk VO_2, V_2O_3, and V_2O_5 at 298 K [63]

Table 1 Photon energies corresponding to the peaks and shoulders as seen in ε_2–E spectra of VO_2 [47]

		Bulk								Film on Al_2O_3			
		$\mathbf{E}\|a$ axis				$\mathbf{E}\perp a$ axis							
Energy (eV)		E_1	E_2	E_3	E_4	E_1	E_2	E_3	E_4	E_1	E_2	E_3	E_4
ε_2	300 K	1.0	1.3	2.6	3.6	0.85	1.3	3.0	3.7	1.0	1.3	2.8	3.5
	355 K	–	–	3.0	3.6	–	0.75	2.9	3.6	–	0.85	2.8	3.5

Table 2 Photon energies corresponding to the peaks and shoulders as seen in ε_2–E spectra of V_2O_3 [52, 53]

Energy (eV)		E_1	E_2	E_3	E_4	E_5	E_6	E_7	E_8
Bulk	148 K	1.0	1.2	2.3	3.0	3.6	4.0	4.5	6.1
Film on Al_2O_3	100 K	–	1.2	2.4	–	–	–	4.6	–
	200 K	–	–	2.0	–	–	–	4.3	–

in the ε_2–E spectra. Clearly, fewer structures are seen in the case of experimental spectra of the thin film as compared to the calculated spectra of the bulk V_2O_3. This can be partially attributed to the optical property calculations combined with other parameters such as temperature difference and possibly surface effects. However, the peaks in insulating phase, existing at three energy locations viz. E_2, E_3, and E_7 (see Table 2), seem to refer to major optical transitions.

Figure 3 shows the dielectric function, reflectivity spectra, and both the real and imaginary part of refractive index of vanadium pentoxide (V_2O_5) from infrared to near-vacuum ultraviolet range (up to 7.0 eV) as a function of temperature below and above T_c. Figure 3a shows the ε_1–E, ε_2–E and R–E spectra of bulk single crystal of V_2O_5 for polarizations parallel to crystallographic axes a, b, and c. The band-edge absorption is visible around 2.0 eV from the ε_2–E spectra, which cannot be described by a unique inter band optical transition but can only be partially attributed to direct forbidden transitions ($\mathbf{k} \neq 0$, where $\mathbf{k}$ is the wave vector) [50]. Beyond the intrinsic edge towards higher energy, the peaks represent the absorption and correspond to electronic transitions from filled 2p (O) to empty 3d (V) states [54]. It can be seen from the ε_2–E and R–E spectra for polarization vector $\mathbf{E}\|a$ axis, in Fig. 3a, that the first sharp absorption occurs at around 2.8 eV, whereas, the second and third peaks appear at 4.3 and 6.4 eV respectively. The dielectric function shows a very high anisotropy in the range between 2.2 and 3.3 eV (visible region) as noticed in ε_1–E and ε_2–E spectra; the spectra in $\mathbf{E}\|a$ axis deviates most from the other two. Clearly, the anisotropy depends on the spatial distribution of electron wave functions and it is possible that the 3d-orbitals directed along the a-axis are relatively more localized, as indicated by narrow intense peak in the ε_2–E spectra for $\mathbf{E}\|a$ axis, forming a wider conduction band. Figure 3b shows the frequency dependent refractive index and extinction coefficient of a polycrystalline thin film of α-V_2O_5 deposited on Al_2O_3 substrate. The measurements were taken from 0.75 to 4.0 eV at various temperatures ranging from 265 to 325 °C, with an increment of 15 °C. Both n–E and k–E spectra exhibit significant temperature dependent change over the entire energy range indicating the phase transition. k–E spectra shows a shift in the absorption edge from 1.5 eV to <0.75 eV as the temperature rises from 280 to 295 °C [7]. The sharp absorption observed in the k–E spectra, at around 3.0 eV, is close to the corresponding absorption peak located at 2.8 eV in bulk V_2O_5.

Application of Penn model

Band structure of a material is related to its R–E spectra (ε_2–E spectra). By definition, an intensity maximum in R (or ε_2) in the R–E spectra (or ε_2–E spectra) represents a maximum number in the optically induced electronic transitions in the material [55]. The energy corresponding to the peak should therefore, correspond to a band-to-band energy difference or a band gap. Since this is a macroscopic gap [44], it should be related to the high-frequency dielectric constant ε_∞ ($=n^2$), where n is the refractive index. It should be noted here that "high-frequency" dielectric constant refers to the "zero-frequency" dielectric constant $\varepsilon(0)$, which is low compared to interband transition frequencies but higher than phonon frequencies.

Several models [44, 56, 57] have been proposed to interpret the frequency and wave-vector dependence of the dielectric function. All these models have, however, been proposed for elemental semiconductors. Extrapolation of the applicability of these models to amorphous semiconductors [58] and narrow and wide gap materials including alkali halides [45, 59, 60] has been carried out with reasonable success. Here, we demonstrate the applicability of one such model to the three oxides of vanadium.

For a model semiconductor, the high frequency dielectric constant is given by [44]:

$$\varepsilon_\infty = 1 + \left(\hbar\omega_p/E_p\right)^2\left[1 - \left(E_p/4E_F\right) + \frac{1}{3}\left(E_p/4E_F\right)^2\right] \quad (3)$$

where, E_p is the Penn gap [44] and E_F is the Fermi energy given by [59]:

$$E_F = 0.2947\left(\hbar\omega_p\right)^{4/3} \quad (4)$$

with the valence-electron plasmon energy given by [61]: $\hbar\omega_p = 28.8(N_v\rho/W)^{1/2}$, W is the molecular weight and N_v is the number of valence electrons per molecule calculated by using:

$$N_v = \mathrm{Ma} + N(8 - b) \quad (5)$$

for a compound A_MB_N, where a(b) is number of valence electrons per atom of type A(B) and M(N) is the atomic fraction of element A(B).

Equation (3) can be rewritten as,

$$\varepsilon_\infty = 1 + \left(\hbar\omega_p/E_p\right)^2 S_0 \quad (6)$$

where, S_0 represents the terms inside the bracket. Since the most significant variation occurs in the expression before S_0, Penn neglects the smaller terms containing E_g/E_F and thus, approximates the value of S_0 as 1 [62]. This is true for materials with band gaps in the commonly occurring range where $E_g/E_F = 0.3$ [57]. However, Grimes and Cowley [57] found that the value of S_0 is only weakly dependent on the band gap and that a value of 0.6 is a fairly good representation of S_0. Thus, with this slightly more accurate value for S_0, the energy gap can be determined by using appropriate values of the dielectric constant.

At room temperature, VO_2 and V_2O_5 are in insulating phase, while V_2O_3 is in metallic phase with very low density of states at the Fermi level [63]. It is believed that IMT is governed by the change in the 3d band structure [64, 65]. In Penn model, the effect of the d band is to increase number of valence electrons per molecule, N_v. Van Vechten [45] has considered, in detail, the effect of d electrons on the dielectric properties of materials. In Table 4, we also evaluate the Penn gap incorporating the d-electron contribution to N_v as indicated within the parenthesis.

It is important to note here that the effective valence–conduction band gap, for the material consisting of different atoms in the unit cell, can be separated into homopolar (E_h) and heteropolar part (C) as introduced by Phillips [66]. Accordingly, we write $E_p^2 = E_h^2 + C^2$ and introduce a parameter, Phillips ionicity, defining ionic character in bonds as $f_i = C^2/\left(E_h^2 + C^2\right)$, where, E_h is related to the static dielectric constant (ε_0) by [46]: $\varepsilon_0 = 1 + \left(\hbar\omega_p/E_h\right)^2 S_0$.

In order to study the Penn gap, which is the macroscopic gap accounting for all the possible optically induced electronic transitions in the material, we rely on the reflectivity data, measured at room temperature, extended for longer range of photon energy as shown in Fig. 4 [63]. Size of the single crystal samples of V_2O_5 and V_2O_3 used in these measurements were $10 \times 10 \times 5$ mm^3 each, whereas, that of VO_2 was $7 \times 5 \times 5$ mm^3. The measurements were performed for the polarization $\mathbf{E}\|a$ axis. The energies corresponding to maxima in intensities seen in Fig. 4 are listed in Table 3.

We can clearly see three major peaks for VO_2 crystal as indicated in the Table. The first peak appearing at 0.7 eV in the insulating phase corresponds to the shoulder appearing

Table 3 Peak energies from reflectivity data of the V–O systems at temperature of 298 K

Energy (eV)	E_1	E_2	E_3	E_4
VO_2	0.7	3.6	7.4	–
V_2O_3	4.2	6.8	9.0	–
V_2O_5	2.97	4.51	6.5	8.1

Table 4 Properties of the V–O systems; the parenthesis value of $\bar{E}$ is the arithmetic average of all the energies corresponding to the peaks and shoulders in the *R–E* spectra

V–O system	Mol. wt (*M*)	ρ (g/cc)	E_g (eV)	N_v	$\hbar\omega_p$ (eV)	E_F (eV)	ε_∞	E_p (eV)	$\bar{E}$ (eV)	ε_0	f_i	*C* (eV)	E_h (eV)
VO_2	82.94	4.68 [69]	0.60 [2]	6	16.56	12.44	9.7 [70]	4.4 (4.6)	3.9 (4.79)	25.9 [70]	0.65	3.55	2.60
V_2O_3	149.88	4.98 [48]	0.66 [41]	10	16.60	12.48	5.0 [71]	6.4 (6.7)	6.6 (6.30)	15.0 [72]	0.71	5.43	3.44
V_2O_5	181.88	3.36 [73]	2.30 [40]	14	14.64	10.55	4.0 [74]	6.5 (6.8)	7.36 (5.52)	13.8 [54]	0.77	5.73	3.17

in the ε_2-E spectra of high temperature phase, in Fig. 1b, both of them having the same origin of transition i. e. from occupied to empty states within the d band [47, 63]. The other two peaks at 3.6 and 7.4 eV refer to the transition from 2p (O) to 3d (V) band. The fact that 3d-band width in V_2O_3 is around 3 eV [65], which is the largest of all three V–O system [63], and the electronic transitions start at 4.2 eV imply that no transition occurs within the d band in V_2O_3. Also, the transitions are mostly to the 4s, 4p bands of vanadium only after 10 eV [63], the observed peaks between 4.2 eV and 9.0 eV can be referred to the transition from 2p (O) to 3d (V) band. We can see four major peaks for V_2O_5 crystal as indicated in the Table and refer to the transition from 2p (O) to 3d (V) band, where the first peak at 2.97 eV shows the highest optical transition rate and is attributed to excitonic transition [63]. Since the first peak appears at relatively high energy, no transition occurs within the d band in V_2O_5.

The results of the calculations based on Penn model are presented in Table 4. Also listed in Table 4, are the values of band gap energy (E_g), zero-frequency (ε_0) and high-frequency (ε_∞) dielectric constants, Phillips ionicity (f_i), average homopolar (E_h) and heteropolar (*C*) energy gaps, Fermi energy (E_F), and arithmetic average of all the energies corresponding to the peaks in the *R–E* spectra ($\bar{E}$). Using the values of E_F and E_p listed in Table 4, we have evaluated the value of S_0 and it is found to be 0.88 which is more than our approximation but still less than unity. It can be seen from Table 4 that the calculated value of E_p for the single crystal of V_2O_3 is close to $\bar{E}$. While E_p of VO_2 and V_2O_5 are also seen to be in good accord with the corresponding values of $\bar{E}$, the difference between E_p and $\bar{E}$ for V_2O_5 is relatively higher as compared to that of VO_2. These relative deviations are consistent with the degree of anisotropy of the three V–O systems. It is important to note here that E_p value of VO_2 and V_2O_3 are closer to the value in the parenthesis (the average of all energies corresponding to the peaks and shoulders in the *R–E* spectra, $\bar{E}$). This indicates that an isotropic, nearly free electron model such as the Penn model seems to be valid in explaining the energies corresponding to the peaks in the reflectivity spectra of these vanadium oxides. It is to be noted here that such a procedure of comparing the calculated E_p with the average of the energies corresponding to the peaks in the *R–E* spectra was proposed by Phillips [46]. Examining the ionicity, we see that the V–O systems are more than 65 % ionic. V_2O_3 and VO_2 follow the general trend that low oxidation states of vanadium oxides are more ionic and undergo IMT [67]. However, V_2O_5 is highly ionic but is consistent with the fact that V_2O_5 is more ionic than VF_5 [68].

Sum rule

At this stage, it would be worthwhile to look into the number of electrons participating in the optical transitions. Most of the electrons in the material are core electrons and are tightly bound to the atomic nuclei. If we consider that the core electrons are excited for high enough frequencies, the sum rule can be written as [75],

$$\frac{2\pi^2 Ne^2}{m} = \int_0^\infty \omega\varepsilon_2(\omega)d\omega \tag{7}$$

where, *m* is the mass of a free electron; *e* the electronic charge; *N* the number of atoms per unit volume (atom density); ω the angular frequency of light, and *n* the total number of electrons per atom. However, the electrons contributing to the optical properties of solids are conduction and valence electrons and, hence, the core states can be neglected. Further assuming that other absorptive processes such as phonon excitation are not overlapping with electronic excitation [76], the effective number of electrons per atom participating in optical transitions over a given frequency range is approximated by,

$$\begin{aligned} n_{eff}(\omega_0) &= \frac{m}{2\pi^2 Ne^2}\int_0^{\omega_0} \omega\varepsilon_2(\omega)\mathrm{d}\omega \ (\textit{In terms of frequency}) \\ n_{eff}(\omega_0) &= \frac{(4\pi\varepsilon_0)m}{2\pi^2 N\hbar^2} \\ &\times \int_0^{E_0} E\varepsilon_2(E)\mathrm{d}E \ (\textit{In terms of Energy and SI system}) \end{aligned} \tag{8}$$

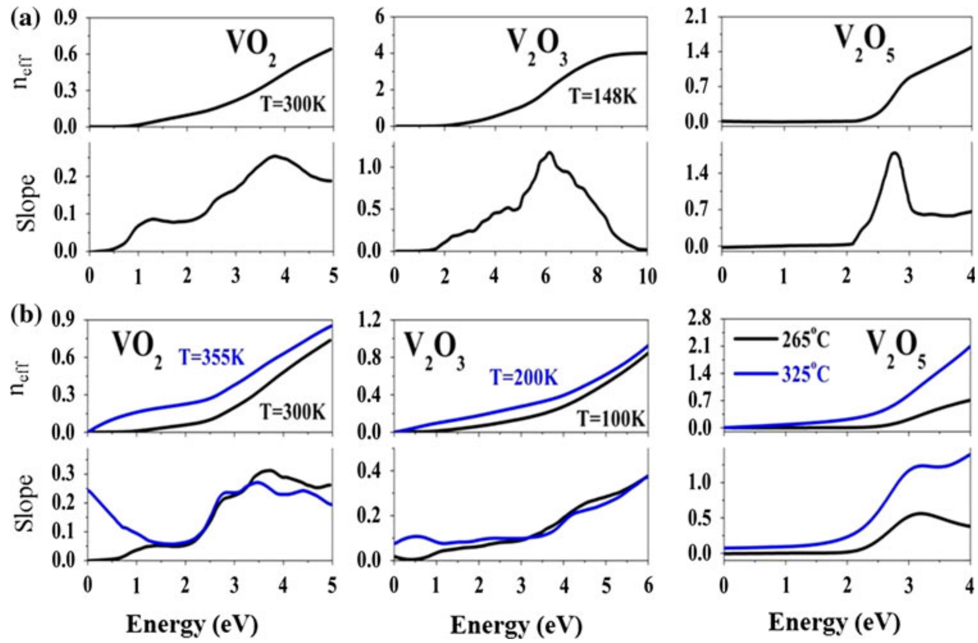

Fig. 5 Variation of n_{eff} with photon energy calculated using Eq. (8) along with its slope with respect to the energy for **a** bulk at polarization **E**||a [47, 50, 52] and **b** film of VO_2, V_2O_3, and V_2O_5 on Al_2O_3 substrate [7, 47, 53] (Color figure online)

where, ε_0 is the permittivity of free space and $n_{eff}(\omega_0)$ is the effective number of electrons per atom governed by polarization of electron shells, contributing to optical transitions below an energy ω_0. Since we are interested in calculating the effective number of electrons per formula unit, we define N as the number of vanadium ions per formula unit per unit volume.

Figure 5 shows the variation of n_{eff} and its slope with photon energy, which were calculated numerically using Eq. (8) for all the three V–O systems at temperatures below and above T_c. The effective number of electrons shows a clear temperature dependent variation with photon energy below and above T_c. The calculated n_{eff} for insulating phase is zero below certain photon energy but varies with photon energy. The rate of change of n_{eff} with respect to energy of incident photons, referred to as slope, is not constant throughout the frequency range and shows significant variation.

The n_{eff} for both the bulk and thin film of VO_2, corresponding to the insulating phase (300 K), is almost zero below 0.6 eV which then varies with the energy of incident photons. The slope for bulk phase, at 300 K, initially increases until 1.2 eV, remains fairly constant from 1.2 to 2.1 eV, rises to a maximum at 3.8 eV, with a small shoulder in between, and finally decreases with increase in photon energy. The region of the shoulder may refer to the transition from 2p (O) to 3d (V) states and is small when compared to its expected value of unity for the absorption due to the one "extra" d electron per formula unit. While there are some differences in the magnitude between the slope of the bulk and film of VO_2, their energy dependent variations show similar pattern. The slope for the high temperature phase of VO_2 initially decreases and reaches minimum at 1.75 eV and then rises until 2.5 eV, and finally shows slight rise and fall alternatively as indicated in Fig. 5b.

The slope for V_2O_3 in Fig. 5a shows the highest peak, besides other small structures, at around 6.1 eV which indicates a strong absorption in the ultraviolet region. This peak is consistent with the corresponding peak in the ε_2–E spectra observed in Fig. 2a. On comparing Fig. 5a, b, we see that the n_{eff} for both the bulk and film of V_2O_3 in its insulating phase show similar trend until 3 eV. However, after 3 eV, the n_{eff} in the film of V_2O_3 deviates considerably from its bulk counterpart, which in fact shows saturation near a value of 4 electrons per formula unit at the end of the ultraviolet spectrum. Assuming that the density functional theory [52] correctly predicts the optical properties of V_2O_3 in the photon energy range of 0–10 eV, this saturation can be attributed mainly to absorption due to the two d-electrons per vanadium ion combined with some contribution due to the transition from 2p (O) to 3d (V) states. However, there is a remarkable difference in the n_{eff} between the bulk and film of V_2O_3 and may require further study to make a definite conclusion to interpret the difference.

The n_{eff} for both the bulk and film of insulating phase of V_2O_5 is almost zero below 2.2 eV and is consistent with the observed absorption band edge. An abrupt change in the slope near the peak region, as seen in Fig. 5a, is characteristic of inter band transition. This peak is consistent with the peak in Fig. 3a in the ε_2–E spectra observed at polarization **E**||a axis. The n_{eff} in bulk phase of V_2O_5 shows a value of 1.49 at photon energy of 4.0 eV. Since V_2O_5 does not have any d electron in its V^{5+} ion, this should be the contribution due to the transition from 2p (O) to 3d (V) states. The value of n_{eff} corresponding to this transition is higher in V_2O_5 as compared to the other two oxides and can be attributed to the higher number of oxygen atoms per formula unit. A similar interpretation can be made for the film of V_2O_5 on Al_2O_3 substrate. However, the variation of n_{eff} with energy at two different temperatures below and above T_c appears to show more consistent pattern at sufficiently high photon energy in both VO_2 and V_2O_3, while a divergence pattern can be easily seen from Fig. 5b for the corresponding variation in V_2O_5. Comparison of n_{eff} of bulk at room temperature and film of V_2O_3 at 265 °C shows different pattern of variation with photon energy which may be partly attributed to the difference in temperature and the highly anisotropic nature of V_2O_5. This may be because studies [2, 7] of optical property do not pertain to the same crystallographic axis besides ambient conditions and other aspects of the experiment, such as the quality of the crystal and analysis procedures. This conclusion is consistent with the perspective of Kang et al. [7], where assertion has been made that the structural phase transition in V_2O_5 does not occur and that V_2O_5 film undergoes an IMT at a critical temperature of 280 °C instead of 257 °C [5] as reported in most of the literature.

Conclusions

Vanadium oxides, which consist of strongly correlated d electrons, are extremely sensitive to the external stimulus such as temperature and undergo insulator–metal transitions (IMT) at a particular temperature depending on the O/V ratio. Vanadium oxides are widely used in technology where devices make use of their properties, such as IMT, high temperature coefficient of resistance (TCR), and a small 1/f noise constant. In this study, we have analyzed the optical properties such as ε_1, ε_2, n, k, and R of bulk and film of VO_2, V_2O_3, and V_2O_5 deposited on Al_2O_3 substrates, based on the data available in the literature. Observed peaks in the corresponding spectra have been interpreted and compared as a function of structure, polarization and temperature. The anisotropy is significant in the infrared region for VO_2 and in the visible region for V_2O_5. Penn model leads to an explanation of the energies corresponding to the peaks in the R–E spectra of the single crystal of the V–O systems at room temperature. E_p values for VO_2 and V_2O_5 are close to the average of energies corresponding to the peaks ($\bar{E}$), while their values are even closer in V_2O_3, clearly reflecting the degree of anisotropy in the order of $V_2O_3 < VO_2 < V_2O_5$. The vanadium oxygen bonds are highly ionic and undergo IMT at T_c as a function of oxidation state of the vanadium ion, i.e., the transition temperature increases with oxidation states of the vanadium atom. Optical transitions and effective number of electrons participating in these processes are described from the ε_2–E spectra and its numerical integration using the well-known sum rule. The results of these calculations show that the optical transitions from valence to conduction band occur including the transition from 2p (O) to 3d (V) bands and the inter band transitions within the d bands. The optical spectra has no indication of the transition occurring from occupied to empty states within the d band for V_2O_3 and V_2O_5 systems but the intra band transition seems to occur in VO_2. The change in n_{eff} with respect to the energy of incident photons is also calculated and it is found that this change is consistent with the peaks observed in the ε_2–E spectra.

Acknowledgements This year marks the 40th anniversary since the publication of Bonds and Bands in Semiconductors by James C. Phillips. The authors dedicate this study to Dr. James C. Phillips and his research group. They thank the Reviewers for their very helpful comments.

References

1. Kotliar G, Vollhardt D (2004) Phys Today 57:53
2. Parker JC, Geiser UW, Lam DJ, Xu Y, Ching WY (1990) J Am Ceram Soc 73:3206
3. Zylbersztejn A, Mott NF (1975) Phys Rev B 11:4383
4. Morin F (1959) Phys Rev Lett 3:34
5. Nadkarni GS, Shirodkar VS (1983) Thin Solid Films 105:115
6. Blum R-P, Niehus H, Hucho C, Fortrie R, Ganduglia-Pirovano MV, Sauer J, Shaikhutdinov S, Freund H-J (2007) Phys Rev Lett 99:226103
7. Kang M, Kim I, Kim SW, Ryu J-W, Park HY (2011) Appl Phys Lett 98:131907
8. Liu W-T, Cao J, Fan W, Hao Z, Martin MC, Shen YR, Wu J, Wang F (2011) Nano Lett 11:466
9. Pergament AL (2011) ISRN Condens Mat Phys 2011:5
10. Lamb DM (2009) Semiconductor to metallic phase transitions from vanadium and titanium oxides induced by visible light. Missouri State University, Springfield
11. Batista C, Ribeiro RM, Teixeira V (2011) Nanoscale Res Lett 6:301
12. Cavalleri A, Tóth C, Siders CW, Squier JA, Ráksi F, Forget P, Kieffer JC (2001) Phys Rev Lett 87:237401
13. Wessel C, Reimann C, Müller A, Weber D, Lerch M, Ressler T, Bredow T, Dronskowski R (2012) J Comput Chem 33:2102
14. Chain EE (1991) Appl Opt 30:2782
15. Dernier PD, Marezio M (1970) Phys Rev B 2:3771
16. Chudnovskiy F, Luryi S, Spivak B (2002) In: Luryi S, Xu JM, Zaslavsky A (eds) Future trends in microelectronics: the nano millennium. Wiley Interscience, New York, p 148
17. Granqvist CG (1985) Phys Scripta 32:401
18. Simic-Milosevic V, Nilius N, Rust H-P, Freund H-J (2008) Phys Rev B 77:125112
19. Kana Kana JB, Ndjaka JM, Owono Ateba P, Ngom BD, Manyala N, Nemraoui O, Beye AC, Maaza M (2008) Appl Surf Sci 254:3959
20. Thomas MS, DeNatale JF, Hood PJ (1997) Mater Res Soc Symp Proc 479:161

21. Zhang Z, Gao Y, Luo H, Kang L, Chen Z, Du J, Kanehira M, Zhang Y, Wang ZL (2011) Energy Environ Sci 4:4290
22. Granqvist CG (1995) Handbook of inorganic electrochromic materials. Elsevier Science, Amsterdam
23. Gupta A, Aggarwal R, Gupta P, Dutta T, Narayan RJ, Narayan J (2009) Appl Phys Lett 95:111915
24. Driscoll T, Kim H-T, Chae B-G, Ventra MD, Basov DN (2009) Appl Phys Lett 95:043503
25. de Almeida LAL, Deep GS, Lima AMN, Neff H (2000) Appl Phys Lett 77:4365
26. Niklaus F, Decharat A, Jansson C, Stemme G (2008) Infrared Phys Technol 51:168
27. Kumar RTR, Karunagaran B, Mangalaraj D, Narayandass SK, Manoravi P, Joseph M, Gopal V (2003) Sens Actuators A 107:62
28. Cole BE, Higashi RE, Wood RA (1998) Proc IEEE 86:1679
29. Driscoll T, Kim H-T, Chae B-G, Kim B-J, Lee Y-W, Jokerst NM, Palit S, Smith DR, Ventra MD, Basov DN (2009) Science 325:1518
30. Driscoll T, Palit S, Qazilbash MM, Brehm M, Keilmann F, Chae B-G, Yun S-J, Kim H-T, Cho SY, Jokerst NM, Smith DR, Basov DN (2008) Appl Phys Lett 93:024101
31. Dicken MJ, Aydin K, Pryce IM, Sweatlock LA, Boyd EM, Walavalkar S, Ma J, Atwater HA (2009) Opt Express 17:18330
32. Kyoung JS, Seo MA, Koo SM, Park HR, Kim HS, Kim BJ, Kim HT, Park NK, Kim DS, Ahn KJ (2011) Phys Status Solidi C 8:1227
33. Hilton DJ, Prasankumar RP, Fourmaux S, Cavalleri A, Brassard D, Khakani MAE, Kieffer JC, Taylor AJ, Averitt RD (2007) Phys Rev Lett 99:226401
34. Baldassarre L, Perucchi A, Nicoletti D, Toschi A, Sangiovanni G, Held K, Capone M, Ortolani M, Malavasi L, Marsi M, Metcalf P, Postorino P, Lupi S (2008) Phys Rev B 77:113107
35. Perucchi A, Baldassarre L, Postorino P, Lupi S (2009) J Phys 21:323202
36. Losurdoa M, Barreca D, Bruno G, Tondello E (2001) Thin Solid Films 384:58
37. Mott NF (1964) Adv Phys 13:325
38. Gunnarsson O (1976) J Phys F 6:587
39. Aurelian C, Julien G, Pierre B, Jean-Christophe O, Corinne C, Alain C (2010). In: Mukherjee M (ed) Advanced microwave and millimeter wave technologies semiconductor devices circuits and systems. In-Tech, Vukovar, Croatia, p 35
40. Scanlon DO, Walsh A, Morgan BJ, Watson GW (2008) J Phys Chem C 112:9903
41. Thomas GA, Rapkine DH, Carter SA, Millis AJ (1994) Phys Rev Lett 73:1529
42. Cardona M (1970) J Res NBS 74A:253
43. Cardona M (1965) J Appl Phys 36:2181
44. Penn DR (1962) Phys Rev 128:2093
45. Van Vechten JA (1969) Phys Rev 182:891
46. Phillips JC (1973) Bonds and bands in semiconductors. Academic Press, New York
47. Verleur HW, Barker AS, Berglund CN (1968) Phys Rev 172:788
48. Zhuze VP, Andreev AA, Shelykh AI (1969) Sov Phys Solid State 10:2914
49. Andrianov GO, Aronov AG, Smirnova TV, Chudnovskii FA (1973) Phys Status Solidi B 60:79
50. Parker JC, Lam DJ, Xu Y-N, Ching WY (1990) Phys Rev B 42:5289
51. Fujiwara H (2007) Spectroscopic ellipsometry: principles and applications. Wiley, New York
52. Guang-Huaa L, Xiao-Yan D, Chun-Hai W (2011) Chin J Struc Chem 30:638
53. Qazilbash MM, Schafgans AA, Burch KS, Yun SJ, Chae BG, Kim BJ, Kim HT, Basov DN (2008) Phys Rev B 77:115121
54. Mokerov VG, Makarov VL, Tulvinskii VB, Begishev AR (1976) Opt Spectrosc 40:58
55. Ravindra NM, Weeks RA, Kinser DL (1987) Phys Rev B 36:6132
56. Breckenridge RA, Shaw RW Jr, Sher A (1974) Phys Rev B 10:2483
57. Grimes RD, Cowley ER (1975) Can J Phys 53:2549
58. Ravindra NM, Narayan J (1986) J Appl Phys 60:1139
59. Ravindra NM, Bhardwaj RP, Kumar KS, Shrivastava VK (1981) Infrared Phys 21:369
60. Kumar A, Ravindra NM (1982) Phys Rev B 25:2889
61. Jackson JD (1978) Classical electrodynamics. Wiley, New York
62. Ravindra NM, Ganapathy P, Choi J (2007) Infrared Phys Technol 50:21
63. Shin S, Suga S, Taniguchi M, Fujisawa M, Kanzaki H, Fujimori A, Daimon H, Ueda Y, Kosuge K, Kachi S (1990) Phys Rev B 41:4993
64. Goodenough JB (1971) J Solid State Chem 3:490
65. Guo Q, Kim DY, Street SC, Goodman DW (1999) J Vac Sci Technol A 17:1887
66. Phillips JC (1968) Phys Rev Lett 20:550
67. Rao KJ, Pecquenard B, Gies A, Levasseur A, Etourneau J (2006) Bull Mater Sci 29:535
68. Malati MA (1999) Experimental inorganic/physical chemistry: an investigative, integrated approach to practical project work. Horwood Publishing, West Sussex, England
69. Donnay JDH (ed) (1963) Crystal data, determinative tables, 2nd edn. American Crystallographic Association, Buffalo
70. Jr Barker AS, Verleur HW, Guggenheim HJ (1966) Phys Rev Lett 17:1286
71. Zhuze VP, Lukirskii DP, Startsev GP (1971) Sov Phys Solid State 13:260
72. Neuberger M (1971) Data compilation on vanadium oxides. Hughes Aircraft Company, Culver City, p 61
73. Kennedy TN, Hakim R, Mackenzie JD (1967) Mat Res Bull 2:193
74. Kenny N, Kannewurf CR, Whitmore DH (1966) J Phys Chem Solids 27:1237
75. Phillip HR, Ehrenreich H (1962) Phys Rev 128:1622
76. Smith DY (1985) Handbook of optical constants of solids. Academic Press, Orlando